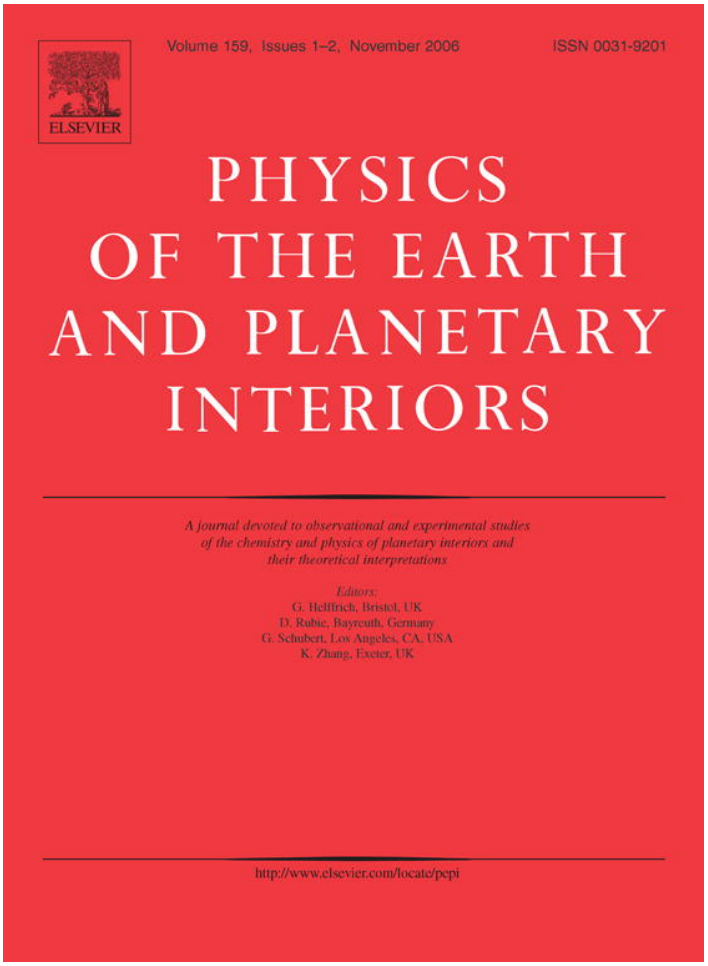

Available online at www.sciencedirect.com
ScienceDirect
Physics of the Earth and Planetary Interiors 159 (2006) 15–31
PHYSICS OF THE EARTH AND PLANETARY INTERIORS
www.elsevier.com/locate/pepi

A new global PKP data set to study Earth's core and deep mantle

R. Garcia [a,*], H. Tkalčić [b,1], S. Chevrot [c]

[a] *Equipe Etudes Spatiales et Planétologie, IPGP, CNRS UMR7154, 4 Ave de Neptune, 94107 St Maur des Fossés, France*
[b] *Atmospheric, Earth and Environment Sciences, Lawrence Livermore National Laboratory, Livermore, CA 94550, USA*
[c] *Dynamique Terrestre et Planétaire, CNRS UMR5562, Observatoire Midi Pyrénées, 31400 Toulouse, France*

Received 16 December 2005; received in revised form 15 May 2006; accepted 15 May 2006

Abstract

We present an extension of the previously developed algorithm for Simulated Annealing Waveform Inversion of Body waves (SAWIB) to resolve the interference between direct PKP seismic phases and their corresponding depth phases (pPKP and sPKP) which occurs for shallow earthquakes. This allows us to process shallow earthquakes previously discarded by the analysts, and therefore improve spatial sampling of the deep Earth by PKP phases. The SAWIB algorithm is applied to available waveform data to determine PKP travel times and amplitudes. The new data set of PKP travel times and amplitudes is significantly larger than previous ones. PKP (bc–df) differential travel time residuals display a hemispherical pattern in the inner core when plotted as a function of the angle between PKPdf propagation direction in the inner core and Earth's rotation axis. Most anomalous differential travel times are along polar paths in the quasi-western hemisphere (180 °W–40 °E), corresponding to earthquakes in the South Sandwich Islands recorded at northern seismic stations. PKP (ab–df) differential travel times display a larger scatter, which we attribute to heterogeneities at the base of the mantle. Relative amplitudes and t^* attenuation parameters are analyzed in terms of inner core attenuation. The inner core attenuation decreases with increasing depth. In the upper inner core, in the depth range 150–220 km, an hemispherical pattern appears with a quasi-western hemisphere (40 °E–180 °E) faster and more attenuating than the rest of the inner core. When stacking PKP waveforms deconvolved by their source time function, we do not find evidence of a global innermost inner core velocity discontinuity. However we cannot rule out the existence of strong local heterogeneities or radial anisotropy variations from our data.

Keywords: Core phases; Seismic waves; Inner Core; Simulated annealing

1. Introduction

Since the early twentieth century, PKP (P′) waves have been used to study Earth's core (Lehmann, 1936; Gutenberg and Richter, 1938). The last two decades have seen an increasing interest in PKP travel times, especially since the discovery that they travel faster along paths that are nearly parallel to Earth's rotation axis (Poupinet et al., 1983; Morelli et al., 1986). Differential PKP travel times were later investigated to reduce the contributions of near source and receiver structures and mislocations in the location of earthquakes (Cormier and Choy, 1986), but also to isolate the contribution of heterogeneities in the lowermost mantle (Sacks and Snoke, 1979; Bréger et al., 1999; Tkalčić et al., 2002) and inner core (Doornbos, 1983; Shearer and Toy, 1991; Creager, 1992; Souriau and Romanowicz, 1996; Tanaka and Hamaguchi, 1997). Theoretical and methodological developments have been achieved recently, with

* Corresponding author. Tel.: +33 1 45 11; fax: + 33 1 45 11.
E-mail address: garcia@ipgp.jussieu.fr (R. Garcia).
[1] Present address: Multimax, Inc., Earth Sciences, 5740 Hollis Street, Emeryville, CA 94608, USA.

0031-9201/$ – see front matter © 2006 Elsevier B.V. All rights reserved.
doi:10.1016/j.pepi.2006.05.003

the finite-frequency Fréchet derivatives of body wave travel times with respect to isotropic phase velocities in isotropic (Dahlen et al., 2000) or transversely isotropic media (Calvet et al., 2006a). This new theory is in principle superior to ray theory because it describes the sensitivity of waves to heterogeneities off the geometrical ray path. However, it requires a precise knowledge of the frequency content of the wave as well as cross-correlation based travel time measurements. These two conditions are not met by current global travel time and amplitude data sets.

In spite of the rapid development of high quality broadband waveform data sets (www.fdsn.org), tomographic studies using PKP data still have to face the problem of uneven sampling of the deep Earth. This problem could be partly overcome if one could make a more complete use of the available data. For example, a method that could deal with the interference of the three PKP branches in the time domain would allow us to use the triplication distance interval 140–149 ° which is usually rejected by the analyst. Such a method has been proposed by Garcia et al. (2004) to treat the seismological records of deep earthquakes at distances close to the triplication. An interesting characteristic of this method is that it extracts the waveforms, in addition to travel times and amplitudes data. Therefore, this approach provides all the seismological observables necessary to fully exploit the resolution potential of finite-frequency tomography based on 3D sensitivity kernels. In the present study, we go one step further and introduce several modifications to our original algorithm to handle the interference between direct and depth phases. This new algorithm allows us to improve the global sampling of the deep Earth by processing shallow events previously discarded because of their complexity. A new data set of PKP absolute and differential travel times and amplitudes is then obtained and compared to previous differential travel time datasets. Finally, we give a preliminary interpretation of our PKP amplitude and travel time measurements in terms of deep Earth structures.

2. Data analysis

2.1. The data set

We analyze vertical component seismograms from the broadband stations of the permanent and temporary networks available through the NetDC data request system, for the time period between 1985 and 2003. The list of seismological networks is given in the acknowledgments section. The data set is subdivided according to the hypocentral depth of earthquakes. For earthquake locations deeper than 90 km, data from all the events with body wave magnitudes larger than 5.7 have been collected. For shallower events, we collected data from events with body wave magnitude larger than 5.8. The larger magnitude threshold for shallow earthquakes accounts for higher attenuation in the upper mantle on the source side. Each record is filtered with a double pass Butterworth Bandpass filter of order 2 in the frequency range 0.3–1.5 Hz. The frequency range is chosen according to the main seismic noise sources. The low cut off frequency is above the double frequency of the microseismic peak (0.125–0.2 Hz), and the high cut off frequency is below the frequency of wind generated noise (2 Hz). After visual inspection we select the seismograms showing clear PKPdf arrivals. This criterium is applied because PKPdf is usually the phase with the smallest amplitude on the records. The number of rejected data is highly dependent on earthquake magnitude, source radiation pattern, and level of microseismic noise at each station. The amount of rejected data is about 10–20% of the total for deep events and 40–50% for shallow events.

2.2. Description of the algorithm

We measure both the amplitudes and travel times of the three PKP phases with the method described in Garcia et al. (2004), hereafter called Simulated Annealing Waveform Inversion of Body waves (SAWIB). The ray paths of the three core phases are plotted in Fig. 1. Our approach consists in a nonlinear inversion of PKP waveforms through a simulated annealing process (Chevrot, 2002). The basic principle is to impose, as an a priori constraint, the relations between the waveforms of the three PKP branches. PKPab is chosen as the reference waveform. PKPbc and PKPdf are then described as Hilbert transforms of the reference waveform. Owing to anelasticity of the inner core, the pulse width of PKPdf

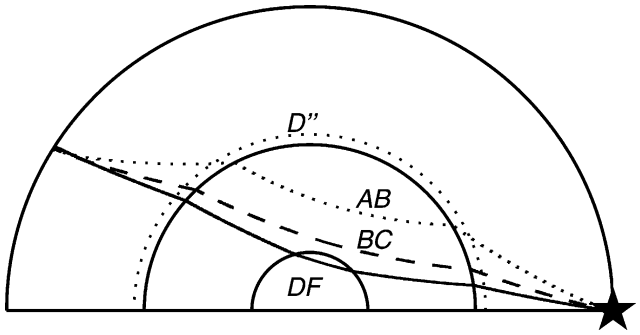

Fig. 1. Ray paths of the three PKP branches: PKPdf (full line), PKPbc (dashed line) and PKPab (dotted line). The event (black star) and the D″ layer at the base of the mantle are also indicated.

is larger than that of PKPab. Thus we introduce an attenuation operator to correct for the differential attenuation of PKPdf relative to PKPab. The amplitudes of the core phases are also corrected for the source radiation pattern, computed from the Harvard CMT solutions (Dziewonski and Woodhouse, 1983), and the geometrical spreading of PKP phases, computed in ak135 reference Earth model (Kennett et al., 1995). After corrections, the waveforms of the three PKP phases should be identical, and we determine the relative travel times and amplitudes between the reference PKPab and the two other phases, PKPdf and PKPbc, when this latter phase is present in the record. The core reflected phase PKiKP is neglected owing to its small amplitude.

2.2.1. Deep earthquakes

For deep earthquakes, each trace $S_i(t)$ is normalized to the maximum amplitude of PKPab and modeled according to:

$$S_i(t) = R_i^{\mathrm{DF}} \times A_i^{\mathrm{DF}} \times A(t_i^*) \times H \times W(t + \tau_i^{\mathrm{DF}}) + R_i^{\mathrm{BC}} \times A_i^{\mathrm{BC}} \times H \times W(t + \tau_i^{\mathrm{BC}}) + W(t + \tau_i^{\mathrm{AB}}) \quad (1)$$

where $S_i(t)$ is the theoretical seismogram recorded by station number i, $W(t)$ is the PKPab reference waveform, $A(t_i^*)$ is a differential attenuation operator, H is the Hilbert transform operator, A_i^{DF} and A_i^{BC} are relative amplitude corrections given by the source radiation pattern and the geometrical spreading of PKP phases, R_i^{DF} and R_i^{BC} are the inverted amplitude parameters, and τ_i^{DF}, τ_i^{BC} and τ_i^{AB} are the inverted time shifts, relative to the beginning of the record, of PKPdf, PKPbc and PKPab phases respectively. The attenuation operator is defined by:

$$A(t^*) = \exp(-\pi f t^*) \exp\left(-2if \ln\left(\frac{f}{f_0}\right) t^*\right) \quad (2)$$

where f is the frequency, and $f_0 = 0.5$ Hz is the reference frequency of PKPdf. This operator assumes a constant Q model, and corrects for the dispersion of PKPdf. The inverted differential travel times depend on the frequency content of the reference waveform without attenuation. The model parameters we invert for are the time samples of the reference waveform $W(t)$, the amplitude corrections R_i^{DF} and R_i^{BC}, the attenuation parameters t_i^*, and the time shifts τ_i^{DF}, τ_i^{BC} and τ_i^{AB}, for each record i.

2.2.2. Shallow earthquakes

In contrast to deep earthquakes, waveform inversion of shallow earthquakes must deal explicitly with the presence of depth phases. For shallow earthquakes (depth smaller than 90 km), each trace $S_i(t)$ is also normalized to the maximum amplitude of PKPab and modeled by:

$$\begin{aligned} S_i(t) = {} & R_i^{\mathrm{DF}} \times A_i^{\mathrm{DF}} \times A(t_i^*) \times H \times W(t + \tau_i^{\mathrm{DF}}) + R_i^{\mathrm{DF}} \times A(t_i^*) \times R_i^{\mathrm{pDF}} \times H \times W(t + \tau_i^{\mathrm{DF}} + \delta t_i^{\mathrm{pDF}}(d)) \\ & + R_i^{\mathrm{DF}} \times A(t_i^*) \times R_i^{\mathrm{sDF}} \times H \times W(t + \tau_i^{\mathrm{DF}} + \delta t_i^{\mathrm{sDF}}(d)) + R_i^{\mathrm{BC}} \times A_i^{\mathrm{BC}} \times H \times W(t + \tau_i^{\mathrm{BC}}) \\ & + R_i^{BC} \times R_i^{\mathrm{pBC}} \times H \times W(t + \tau_i^{\mathrm{BC}} + \delta t_i^{\mathrm{pBC}}(d)) + R_i^{\mathrm{BC}} \times R_i^{\mathrm{sBC}} \times H \times W(t + \tau_i^{\mathrm{BC}} + \delta t_i^{\mathrm{sBC}}(d)) \\ & + W(t + \tau_i^{\mathrm{AB}}) + R_i^{\mathrm{pAB}} \times W(t + \tau_i^{\mathrm{AB}} + \delta t_i^{\mathrm{pAB}}(d)) + R_i^{\mathrm{sAB}} \times W(t + \tau_i^{\mathrm{AB}} + \delta t_i^{\mathrm{sAB}}(d)) \end{aligned} \quad (3)$$

where R_i^{pDF}, R_i^{sDF}, R_i^{pBC}, R_i^{sBC}, R_i^{pAB} and R_i^{sAB} are the relative amplitudes of depth phases with respect to the reference phase. Differential times δt between direct and depth phases are computed for a particular hypocentral depth d. Hypocentral depth is refined by exploring a depth interval of ±20 km around the hypocentral depth given by Engdahl et al. (1998) relocations. In addition to the parameters inverted for deep earthquakes, we thus also invert for the depth of the earthquake and relative amplitude parameters between the depth phases and the reference direct phase.

2.2.3. Minimization of the misfit function by simulated anealing

For both deep and shallow earthquakes, we explore the epicentral distance range 145–176° in which the PKP phases are recorded. The PKPbc waveform is modeled only in the 145–153.5° distance range, because at larger epicentral distances its waveform is distorted by diffraction at the inner core boundary.

All the PKP records in the selected epicentral distance range for each earthquake are inverted simultaneously. Since we take into account the source radiation pattern, we are able to analyze the records for all azimuths simultaneously.

A L1 norm misfit between data and synthetics is minimized by simulated annealing. The simulated annealing algorithm is a Monte Carlo Markov Chain algorithm with the probability of uphill investigation of the misfit function decreasing during the cooling schedule (Sen and Stoffa, 1995; Sharma and Kaikkonen, 1998; Kolář, 2000; Chevrot, 2002; Garcia et al., 2004). An exponential cooling schedule (Salamon and Berry, 1983; Nulton and Salamon, 1988; Andresen and Gordon, 1994) of the form $T(k) = \gamma^k T(0)$ is implemented with $\gamma = 0.992$ and $N = 1500$ iterations. The starting temperature $T(0)$

is fixed at one tenth the value of the initial misfit in order to start well above the critical temperature of the system, and $T(1500) \approx 5.8 \times 10^{-6}\, T(0)$. The initial reference waveform is the stack of all the records of the reference phase. The initial time shifts are the theoretical shifts computed in the ak135 reference model. The attenuation parameters are set to 0.4 s, and the amplitudes parameters of the direct phases are set to one. For shallow earthquakes, the initial hypocentral depth is taken from Engdahl et al. (1998) relocations, and the amplitude parameters of the depth phases are set to 0.1 in order to allow the convergence of the direct phases before the depth phases. However, the starting values of the parameters are not critical because the simulated annealing process explores rapidly the parameter space at the beginning of the cooling process. At each temperature step, 10 random perturbations are implemented for each parameter. The reference waveform and amplitude parameters are perturbed by increments of 1% of the maximum amplitude, and only perturbations that decrease the misfit function are accepted. For time shifts, attenuation parameters, and event depths, perturbations are random in a predetermined range, and are accepted according to a Boltzmann statistics depending on misfit change and temperature $T(k)$. The model giving the lowest misfit value during the simulated annealing process is chosen as the best model.

2.3. Error estimates

The simulated annealing inversion is repeated six times with different seeds for the random number generator and the variance of the output parameters over the six runs is computed. This variance is called "statistical error", and gives an indication of the convergence of the algorithm. If the inversion is stable and always converges towards the same minimum, this error will be zero for all the parameters. On the other hand, if this error is large for one parameter, this means that the misfit function has secondary minima of about the same amplitudes, but which are far from each other in the model space. In such cases, usually resulting from poor signal to noise ratio in the records, travel time measurements are unreliable, and therefore they are rejected for standard deviations above 0.5 s.

In addition to the statistical error, two other measures of the results reliability are estimated. First, the L1 norm signal to noise ratio (SNR) of each phase is computed by dividing the L1 norm of the synthetic waveform by the L1 norm of the noise which is estimated by taking a similar time window 8 s before the PKPdf arrival. High signal to noise ratios are more likely to give reliable measurements of amplitude and travel times. Finally, the cross-correlation error (CCE) is defined for each time shift τ_i^{DF}, τ_i^{BC} and τ_i^{AB} by measuring the half-width of the cross-correlation peak between the synthetic waveform and the record (Chevrot, 2002). Whereas the statistical error of the time shift gives an indication of the stability of the inversion process, the cross-correlation error estimates the error in travel time resulting from waveform distortion. Analyzed simultaneously, these error estimates quantify the quality and reliability of the measurements, and allow us to clean the database by excluding outliers and poorly constrained measurements.

2.4. Examples

Previous studies focused on catalog based lower quality travel time measurements or on high quality handmade differential travel time measurements with well-separated PKP arrivals and depth phases. Unfortunately, such records are scarce, especially for shallow sources. In addition, the complexity in the triplication range often precludes measurements of absolute and differential travel times, especially when data were recorded by a small number of stations.

2.4.1. Resolving the interference within the triplication range

One of the main advantages of SAWIB over commonly used cross-correlation methods resides in its ability to retrieve waveforms and differential travel times of PKP phases at epicentral distances close to the PKP triplication, where all three PKP arrivals interfere. Fig. 2a illustrates this property by showing the final waveform fit for the deep, 29 March 1998, Fiji earthquake. In this time–distance plot, the synthetic waveforms predicted by the values of the parameters giving the smallest misfit are compared to the data after alignment on the PKPab phase. At large epicentral distances, the different core phases are clearly separated in time. A good data fit is achieved in the whole distance range, which suggests that the inversion is indeed able to resolve the interference close to the triplication.

2.4.2. Resolving the interference between direct and depth phases

Another important advantage of SAWIB is its ability to simultaneously resolve the travel times and amplitudes of both direct and depth phases. This allows us to analyze numerous shallow earthquakes which were rejected in previous PKP studies, owing to the complexity of the records. Fig. 2b and c illustrate a waveform fit for a 54 km deep earthquake, which occurred on 18 June 2002, near

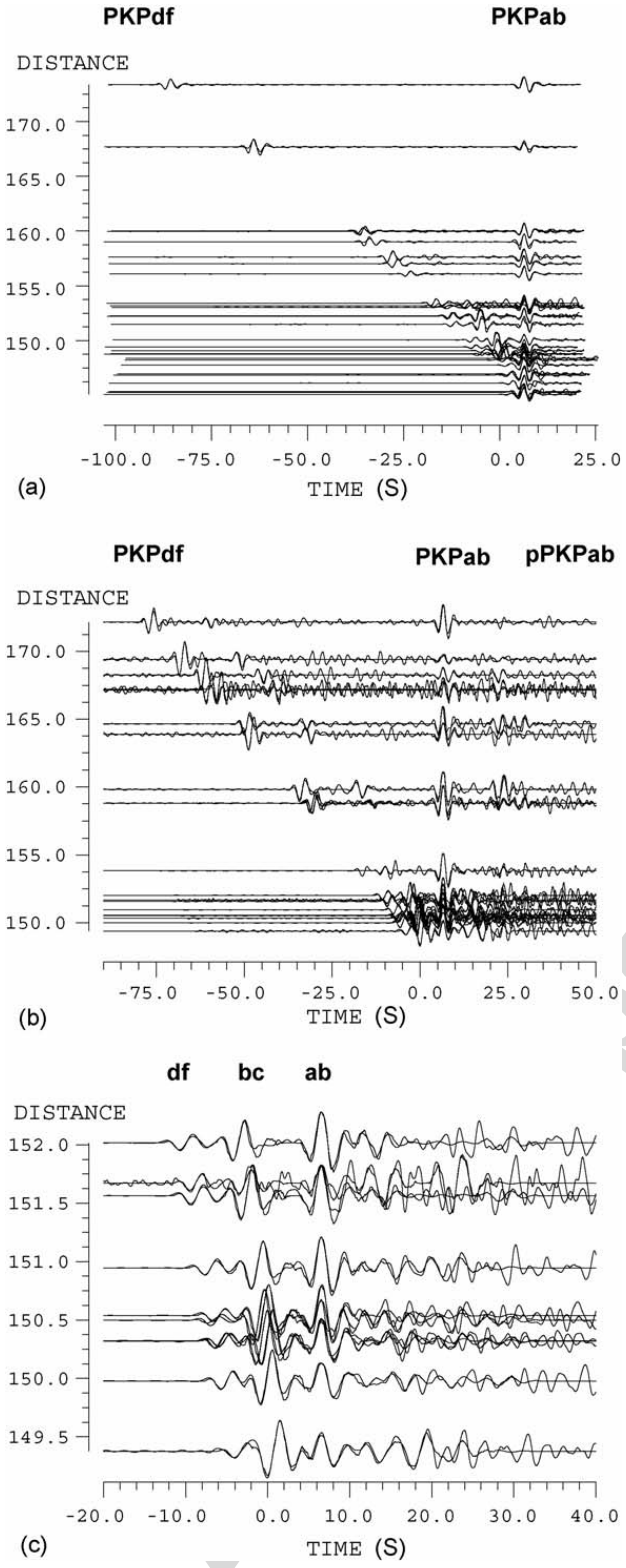

Fig. 2. Examples of waveform fit for (a) a deep earthquake (535 km depth) and (b) a shallow earthquake (54 km depth). The traces are aligned on the PKPab reference waveform arrival. Waveforms (thick lines) and synthetic (thin lines) traces are plotted on the record sections with respect to the epicentral distance (in degrees). (c) is a zoom of (b) close to the triplication.

the coast of central Chile. At large epicentral distances, the phases are clearly separated and properly fit both in time and amplitude. Close to the PKP triplication (Fig. 2c), the direct and depth phases strongly interfere, and any measurement procedure based on cross-correlation would clearly fail. Yet, our method is able to resolve this interference pattern and determine the travel times and amplitudes of the different phases.

3. The new data set

3.1. Description

The database, obtained after inversion of all the broadband PKP records available through NetDC at IRIS, is composed of 4463 traces for deep earthquakes and 7595 traces for shallow earthquakes. Fig. 3 presents histograms of PKP (ab–df) differential travel time statistical errors and PKPdf signal to noise ratio for deep and shallow events. For deep events, about 65% of the differential travel time estimates are stable in the inversion process and the corresponding signal to noise ratio has a peak around 0.8. For shallow events, only about 30% of the differential travel time estimates are stable, owing to a poor PKPdf signal to noise ratio. For the same magnitude, the amplitude of PKPdf phase is smaller for shallow earthquakes than for deep earthquakes owing to anelasticity of the upper mantle. The source time functions are usually more complex for shallow events. In addition, crustal heterogeneities close to the source introduce waveform distortions of the depth phases which vary with azimuth. In order to avoid false detections, we select the data with a differential travel time statistical error less than 0.5 s, and a signal to noise ratio greater than 2.5 for both the reference phase (PKPab) and PKPdf. Despite these criteria, misidentifications of phases are still possible, for example by fitting PKPbc waveform with synthetic PKPdf phase. Such errors produce strong outliers easily detectable by eye. Therefore, the data resulting in differential travel time residuals PKP (ab–df) and PKP (bc–df) outside the ± 3 and ± 5 second windows, respectively, are visually checked upon which the resulting misidentifications of core phases are removed. These data represent about 2% of the initial data set. The remaining data base is composed of 1802 traces for deep earthquakes and 1247 traces for shallow earthquakes.

3.2. Sampling of the inner core and D″

In the following, the deep Earth coverage by our data set is compared to the coverage of Tkalčić et al. (2002) who assembled, at the time, the most comprehensive

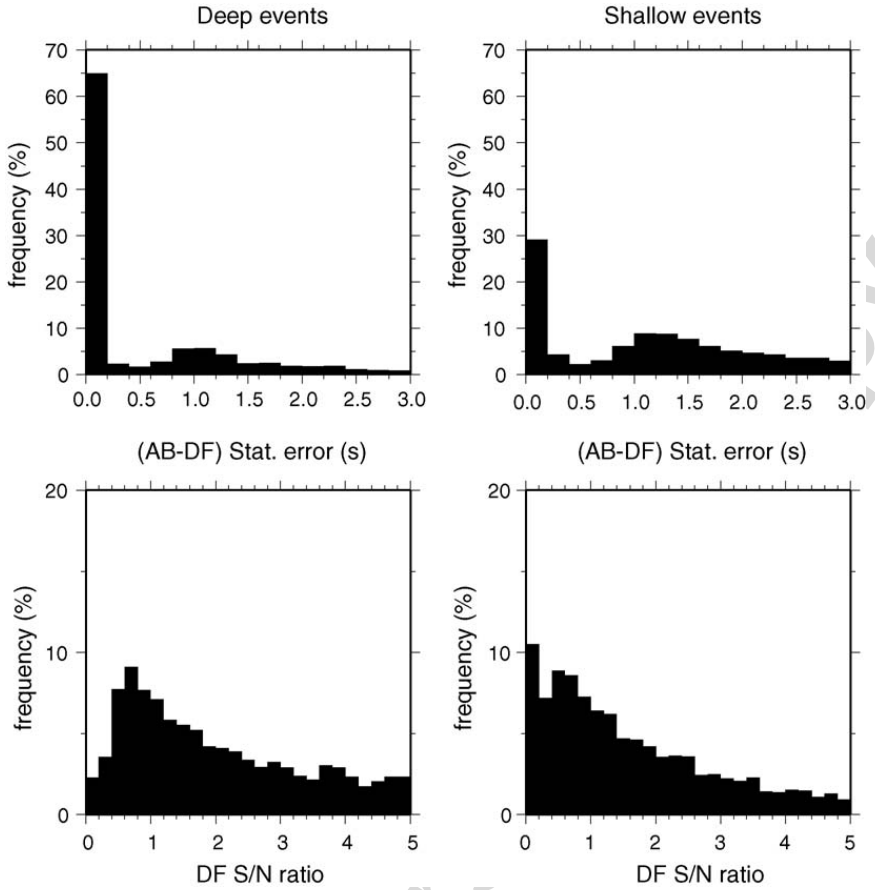

Fig. 3. Histograms of PKP (ab–df) differential travel time statistical errors (top panels) and PKPdf signal to noise ratio (bottom panels) for deep events (on the left) and for shallow events (on the right).

collection of high quality hand-picked and cross-correlation based PKP travel time residuals. Their dataset is a collection of PKP differential travel times measured by four independent groups of researchers. Fig. 4a and b illustrates the improvement in spatial sampling of the inner core achieved by adding shallow earthquakes to the deep ones. This improvement is very important for the lowermost mantle and core studies. Indeed, previous studies relied almost exclusively on deep earthquakes. In addition to a global increase of the data set for subduction events, shallow earthquakes, originating from oceanic ridges in the Indian ocean and regions surrounding Antarctica, sample new paths in the lower mantle and the inner core below the Indian and Pacific oceans. The new inner core coverage in Fig. 4b is compared to the 2002 coverage shown in Fig. 4c. The two data sets look very complementary because they have been constructed with different objectives. The older data set has been collected to constrain specific structures of the inner core and the lowermost mantle, with a significant number of data extracted from specific networks. As a result, some ray-paths in the inner core nearly parallel to Earth's rotation axis are over-represented. In contrast, our data set is more evenly distributed at the global scale, but less specifically focused on paths sampling particular deep Earth structures. The sampling and azimuthal coverage is improved below the Pacific ocean and the southern hemisphere.

Fig. 5 illustrates the improvement in spatial sampling of the lowermost 300 km of the mantle achieved in this study relative to the 2002 coverage. The common feature in both data sets is a poor sampling of the lowermost mantle below Africa and south of Indian ocean. However, sampling of the lowermost mantle is improved by shallow events below the Atlantic and Pacific oceans.

3.3. Travel times and reference Earth model

In the pre-processing stage, the onset of the reference phase is manually picked on a chosen good quality record for each event. By using this absolute travel time and the differential time shifts obtained by the inversion, the absolute travel times of all the core phases are determined for each event.

Fig. 6a shows absolute travel time residuals with respect to Earth reference model ak135 as a function of

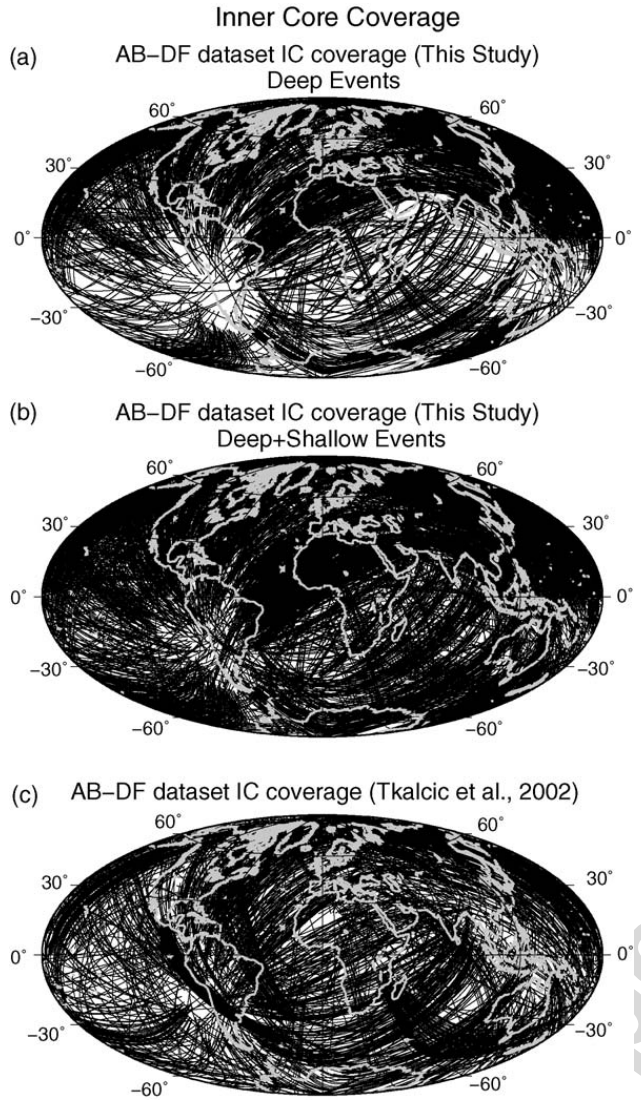

Fig. 4. Projection on Earth's surface of the PKPdf inner core paths for deep earthquakes (a), for both deep and shallow earthquakes (b), and for Tkalčić et al. (2002) data set (c).

epicentral distance. The average value and the trend of absolute residuals as a function of epicentral distance for the three core phases are in good agreement with ak135.

Fig. 6b shows the differential travel times of core phases with respect to ak135 model. The average differential travel time residuals are close to zero, and in excellent agreement with ak135. The standard deviation of the differential travel time residuals is larger for differential travel times involving PKPab phase due to the significantly different ray paths between PKPab phase and the other two core phases, and due to the larger sensitivity of PKPab travel time to D″ heterogeneities. The PKP (ab–df) differential travel time residuals present a small trend of decreasing residuals with increasing epicentral distance. This feature is compatible with the slight trend seen in PKPdf absolute travel times and reveals a small overestimate of seismic velocities in the deeper parts of the inner core.

3.4. Comparison with previous studies

We now compare our newly assembled differential travel time dataset with the dataset described in Tkalčić et al. (2002), in which the most anomalous observations are predominantly related to a very specific group of paths from the South Sandwich Islands to North America and North Asia.

Fig. 7 shows PKP (bc–df) differential travel time residuals, calculated with respect to the reference model ak135 (Kennett et al., 1995), as a function of (a) the angle ξ (the angle between a PKPdf leg in the inner core and Earth's rotation axis) and (b) the epicentral distance. The residuals corresponding to PKPdf bottoming in the quasi-eastern hemisphere of the inner core are shown by "plus" symbols while those corresponding to the quasi-western hemisphere by circles, following the definition of the hemispheres given by Tanaka and Hamaguchi (1997). Equivalent plots from PKP (bc–df) dataset from Tkalčić et al. (2002) are shown in (c) and (d). For both data sets, average PKP (bc–df) residual is about 0.5–1.0 s larger for the eastern hemisphere than for the western hemisphere data. Moreover, in panel 7b, the difference between hemispherical averages of PKP (bc–df) residuals appears to decrease with increasing distance. This result suggests that the hemispherical pattern of upper inner core velocities disappears progressively at larger depths in the inner core (Wen and Niu, 2002; Garcia, 2002; Cao and Romanowicz, 2004). In spite of the low number of polar data ($\xi < 35^\circ$) in our data set, a similar distinction between an anisotropic western hemisphere and an isotropic eastern hemisphere is observed (Tanaka and Hamaguchi, 1997). In both data sets, the anomalous polar data are associated with a particular path from the South Sandwich events to the northern stations of America.

Fig. 8 shows PKP (ab–df) differential travel time residuals as a function of (a) the angle ξ and (b) the epicentral distance. Same plots of PKP (ab–df) from Tkalčić et al. (2002) are shown in (c) and (d). In contrast to PKP (bc–df) residuals, a large scatter of PKP (ab–df) residuals is observed, as in previous studies (Bréger et al., 2000). This scatter can be assigned to strong lower mantle heterogeneities influencing PKPab, which is slightly larger in our data set than in Tkalčić et al. (2002). This difference can be explained by the addition of shallow data that experience more small scale heterogeneities in the upper mantle on the source side. For the polar data ($\xi < 35^\circ$), the most anomalous residuals correspond to ray paths in

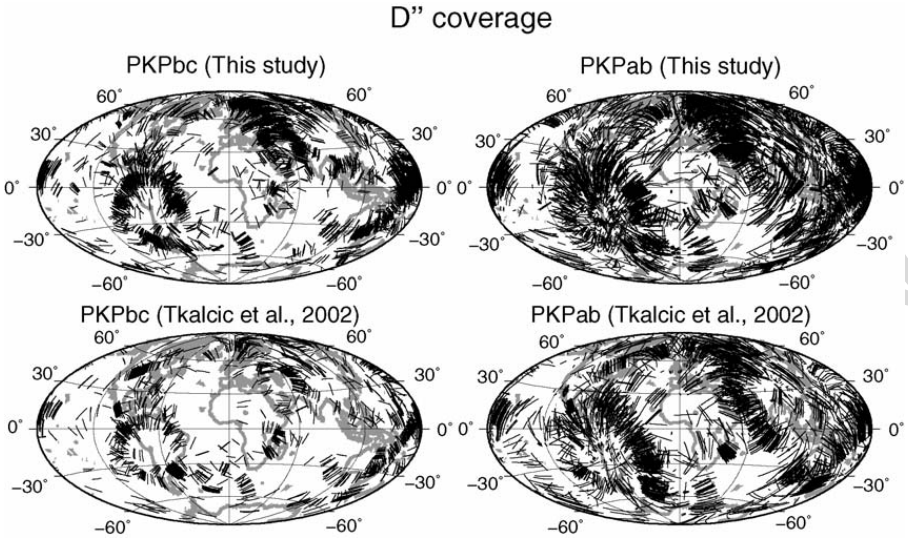

Fig. 5. (a) Projection on Earth's surface of the PKPbc (left) and PKPab (right) rays paths in the last 300 km of the mantle for our data set (top) and Tkalčić et al. (2002) data set (bottom).

the western hemisphere associated with the South Sandwich events which are clearly seen as a cluster of large positive PKP (ab–df) residuals. However, due to a large scatter of PKP (ab–df) residuals, the hemispherical pattern of inner core anisotropy is less clearly visible than for PKP (bc–df) residuals.

4. Heterogeneities in the lowermost mantle

The differential travel time residuals of core phases are sensitive to the lowermost mantle structure because each core phase samples different regions of the lowermost mantle both on source and receiver sides. This

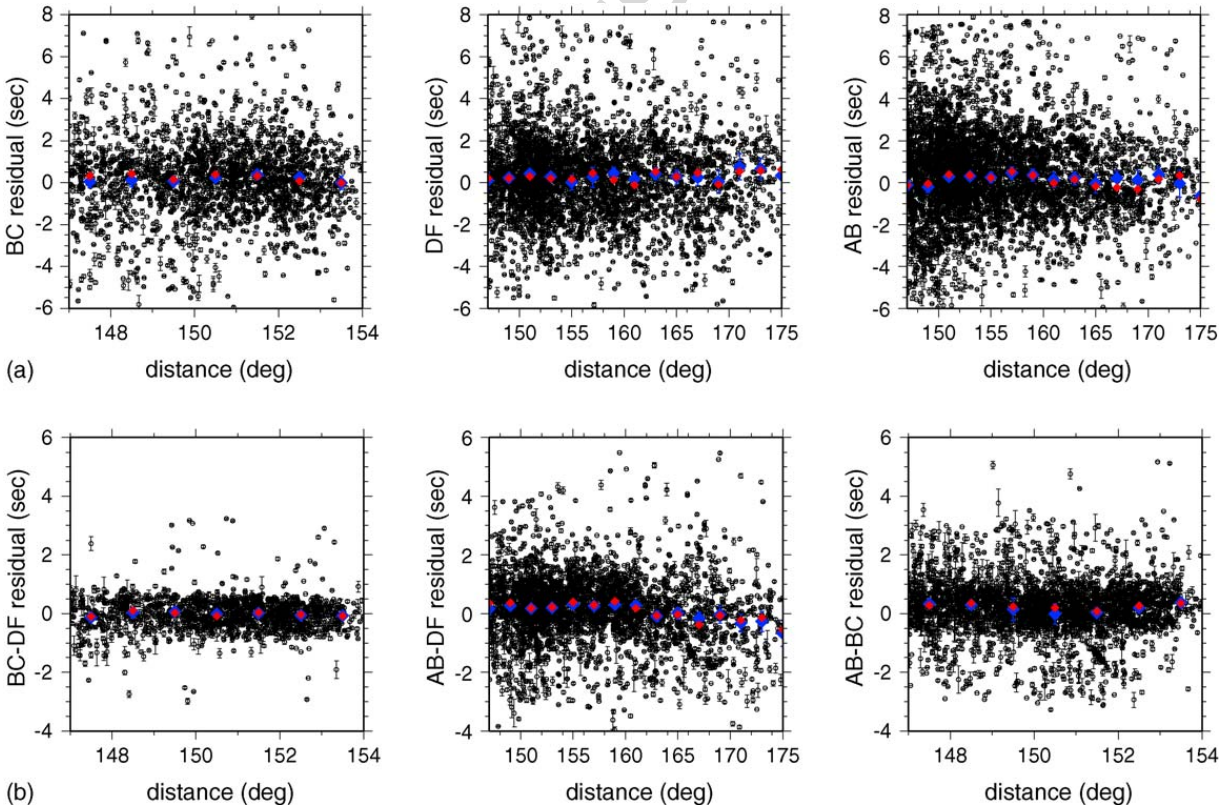

Fig. 6. (a) Absolute travel time residuals (in s) as a function of epicentral distance (in degrees) of PKPbc (left), PKPdf (middle) and PKPab (right). (b) differential travel time residuals (in s) as a function of epicentral distance (in degrees) of PKP (BC–DF) (left), PKP (AB–DF) (middle) and PKP (AB–BC) (right). Black dots represent individual measurements, red and blue diamonds represent median and average values in epicentral distance bins, respectively. All the residuals are computed relative to ak135 Earth model and 2σ errors bars are plotted for average values.

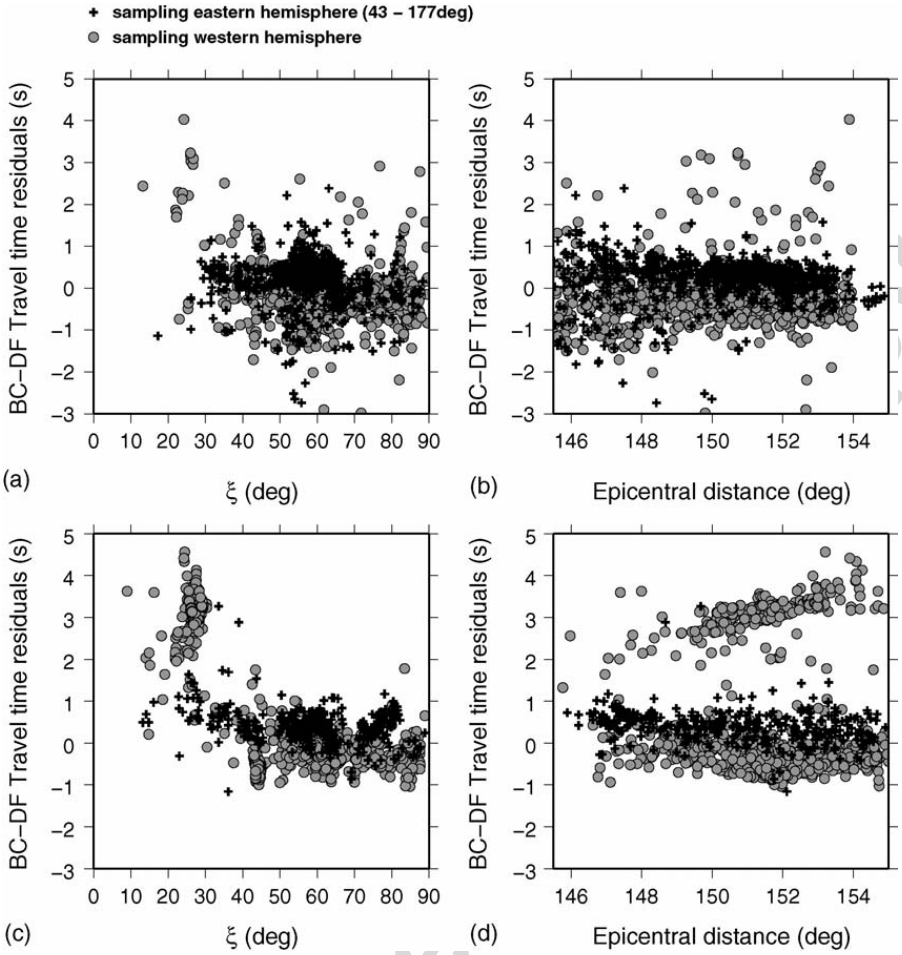

Fig. 7. Comparison between our PKP (bc–df) differential travel time data set (a and b) and Tkalčić et al. (2002) one (c and d). On the left, travel time residuals are plotted as a function of the angle ξ between PKPdf leg in the inner core and Earth's rotation axis (a and c), and on the right, as a function of the epicentral distance (b and d). Crosses and circles stands for data with PKPdf bottoming point respectively in a quasi-eastern (40–180 °E) and a quasi-western hemisphere.

effect is particularly important for PKP (ab–df) residuals at large epicentral distances because the lowermost mantle ray paths of PKPdf and PKPab are separated by about 15°, and because PKPab has a grazing incidence at the core-mantle boundary. The prevailing effect of lowermost mantle heterogeneities on PKPab travel times is illustrated by the scatter of PKP (ab–df) residuals (Fig. 8) which is about two times larger than the scatter of PKP (bc–df) residuals (Fig. 7) at the same epicentral distance. The observed differential travel time scatter gives us an indication of the magnitude of small-scale velocity variations in the lowermost mantle. Relative differential travel time anomalies as large as 0.7 s over lateral distances as small as 2.5° at the core surface have already been observed (Garcia et al., 2004). Fig. 9 shows the PKP (ab–df) and PKP (bc–df) residuals plotted at both core entry and exit points of PKPab and PKPbc, respectively. The map shown in Fig. 9 also illustrates well the lowermost mantle coverage (see also Fig. 5). Strong, small scale variations are observed in many places, which suggest the presence of small scale structures in the D″ region (Garnero et al., 1998; Bréger et al., 1999; Garnero and Jeanloz, 2000; Tkalčić et al., 2002; Ni et al., 2002). The ambiguity between the D″ structure at the source and at the receiver sides can only be resolved by a global inversion including not only core phases, but also mantle phases. Since differential travel times do not constrain long wavelength structure of the lowermost mantle but the velocity gradients, only a joint inversion of both absolute and differential travel times can fully resolve the structures in D″. This will be the objective of a forthcoming study.

5. Inner core structure

5.1. Hemispherical pattern and anisotropy

Figs. 7 and 8 suggest a hemispherical pattern of inner core anisotropy. However, the large scatter of PKP (ab–df) residuals also indicates a strong influence of

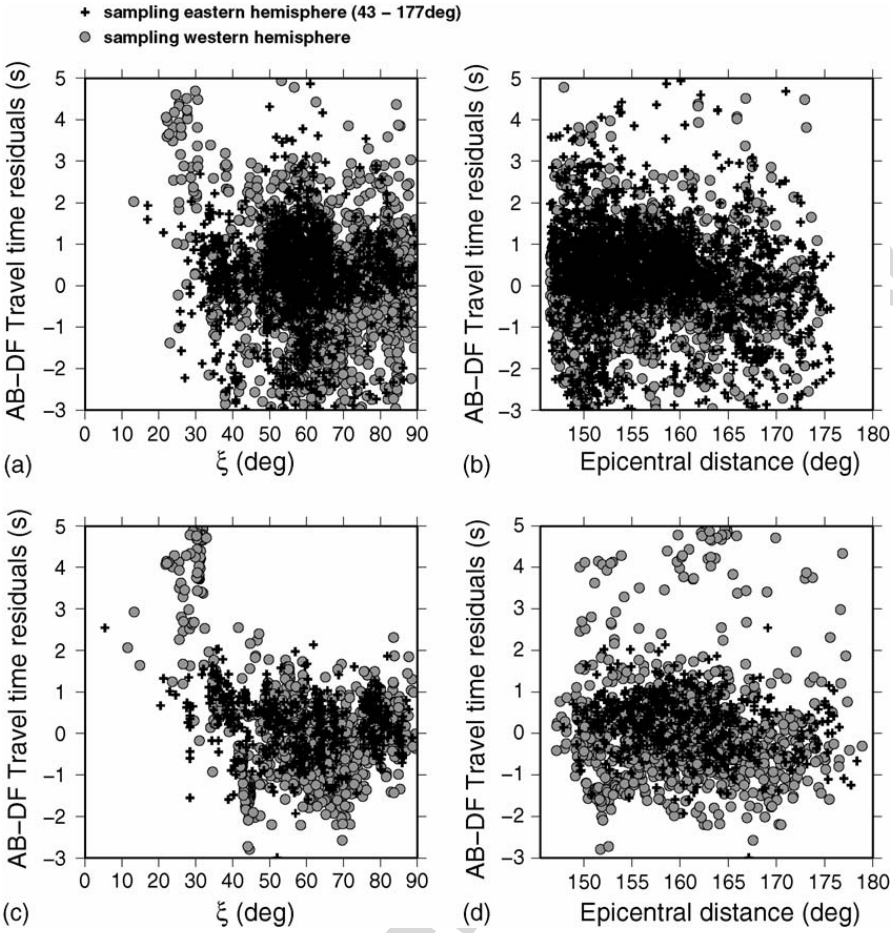

Fig. 8. Comparison between our PKP (ab–df) differential travel time data set (a and b) and Tkalčić et al. (2002) one (c and d). On the left, travel time residuals are plotted as a function of the angle ξ between PKPdf leg in the inner core and Earth's rotation axis (a and c), and on the right, as a function of the epicentral distance (b and d). Crosses and circles stands for data with PKPdf bottoming point respectively in a quasi-eastern (40–180 °E) and a quasi-western hemisphere.

lowermost mantle heterogeneities. Consequently, PKP (ab–df) residuals are not further considered in the discussion of inner core anisotropy effects on differential travel time residuals. Fig. 10 presents the geographical distribution of the polar PKP (bc–df) residuals ($\xi < 35^\circ$) and further enhances the effect of anomalous residuals from the South Sandwich events. The data are plotted with (top) and without (bottom) data from events in the South Sandwich subduction zone. As can be seen, the hemispherical pattern of inner core anisotropy is much less pronounced when the South Sandwich data are removed from the plot. Moreover, some data from shallow events sample approximately the same ray path, but they do not exhibit large positive PKP (bc–df) residuals. This result illustrates the improvement obtained by adding data from shallow events. Because of the unique amplitude of the anomaly of PKP (bc–df) polar residuals for the South Sandwich events, heterogeneities along this path must be strong and have a very specific geometry (Romanowicz et al., 2003). All these results justify the need to increase the coverage of the core phases data set by adding shallow event data, and the necessity to invert simultaneously core and mantle structures.

5.2. Inner core attenuation

The attenuation of PKPdf is described in the inversion by the attenuation operator $A(t^*)$. The parameters t_i^* and R_i^{DF} are correlated owing to the influence of attenuation on both the amplitude and the phase of PKPdf. This correlation makes it difficult to measure the t_i^* parameters independently. Accordingly, inner core is characterized by looking simultaneously at t_i^* and at the products $\mathrm{DF/AB} = \exp(-\pi f_0 t_i^*) \times R_i^{\mathrm{DF}}$ and $\mathrm{DF/BC} = \exp(-\pi f_0 t_i^*) \times R_i^{\mathrm{DF}}/R_i^{\mathrm{BC}}$ which include attenuation effects at reference frequency $f_0 = 0.5$ Hz. DF/BC and DF/AB amplitude ratios corrected for geometrical spreading and source radiation pattern are plotted in Fig. 11, in addition to t_i^* parameter, as a function of

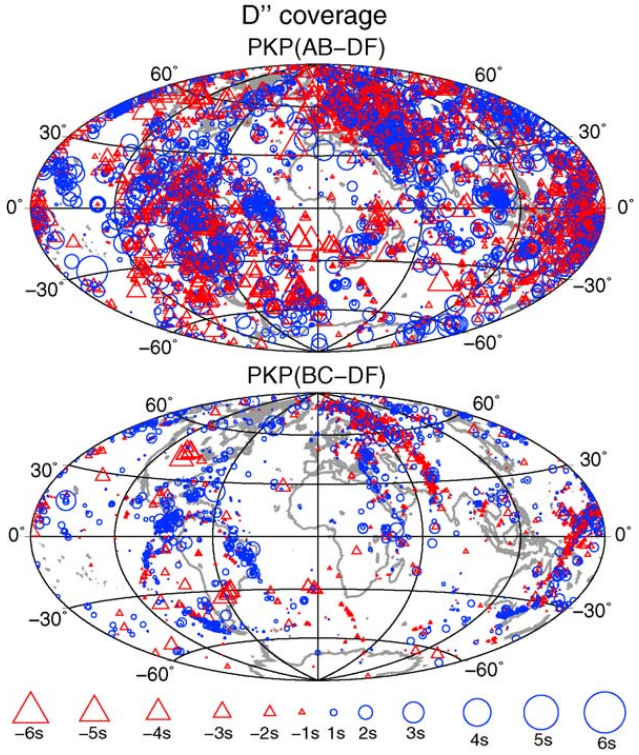

Fig. 9. Differential travel time residuals PKP (ab–df) (top) and PKP (bc–df) (bottom) respectively plotted at both core entry and exit of PKPab and PKPbc phases. Symbol color and size is referred to the amplitude of the residual.

parameters describing the geometry of the rays. DF/BC amplitude ratios, presented on panels (a) and (b), show a V shape resulting from the influence of two competing effects. When the epicentral distance is smaller than 150°, the DF/BC ratio decreases with increasing distance owing to inner core attenuation (Fig. 11b). When PKPbc turning point radius is deeper than 1400 km (Fig. 11a), DF/BC amplitude ratio increases as the turning point of PKPbc approaches inner core boundary. This results from a decrease of the PKPbc amplitude produced by finite frequency diffraction at the inner core boundary (Cormier and Richards, 1977). A 2 s period PKPbc begins to be sensitive to the inner core boundary about 200 km above it.

In order to model this effect, we have computed full wave theory synthetic seismograms (Cormier and Richards, 1977) in the spherically symmetric model ak135 including inner core attenuation. The synthetic seismograms were then filtered and inverted with SAWIB following the same procedure as for real data. The waveform fit is shown in Fig. 12 and the measured amplitude ratios are plotted in Fig. 11 (red line). An important consequence of PKPbc diffraction is that DF/BC amplitude ratios are biased at low frequencies for epicentral distances greater than 150°. Such a result questions the validity of the spectral ratio method at low frequencies (Niazi and Johnson, 1992; Bhattacharyya et al., 1993; Souriau and Roudil, 1995; Helffrich et al.,

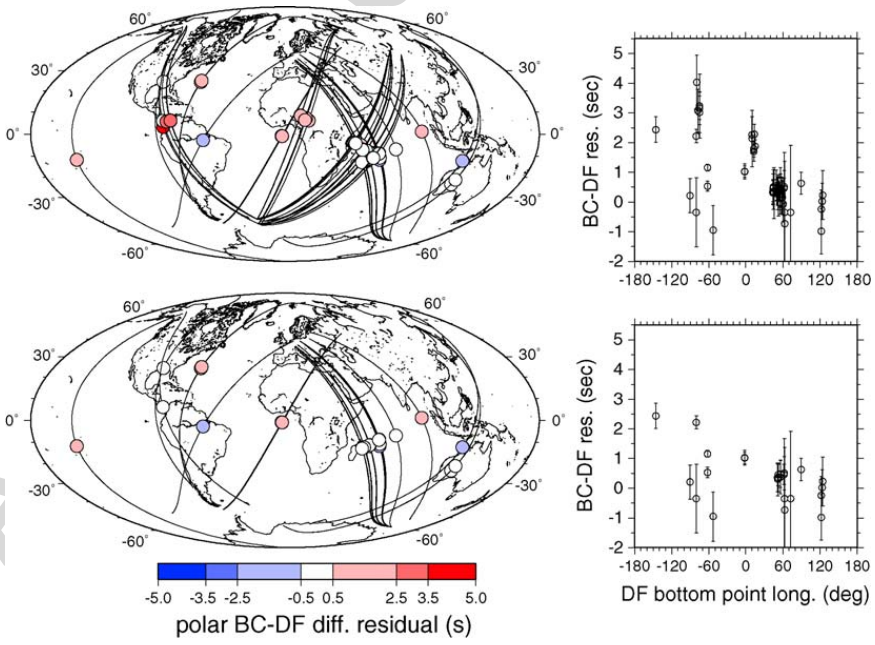

Fig. 10. PKP (bc–df) polar ($\xi < 35°$) differential travel time residuals plotted as a function of the PKP (DF) turning point (left) and as a function of the PKP (DF) turning point longitude (right). At the top, the whole data set of polar PKP (bc–df) differential travel time residuals is plotted. At the bottom, the data from South Sandwich events have been excluded. Error bars are the sum of the cross-correlation error estimates of each core phase used for the computation of the differential travel time.

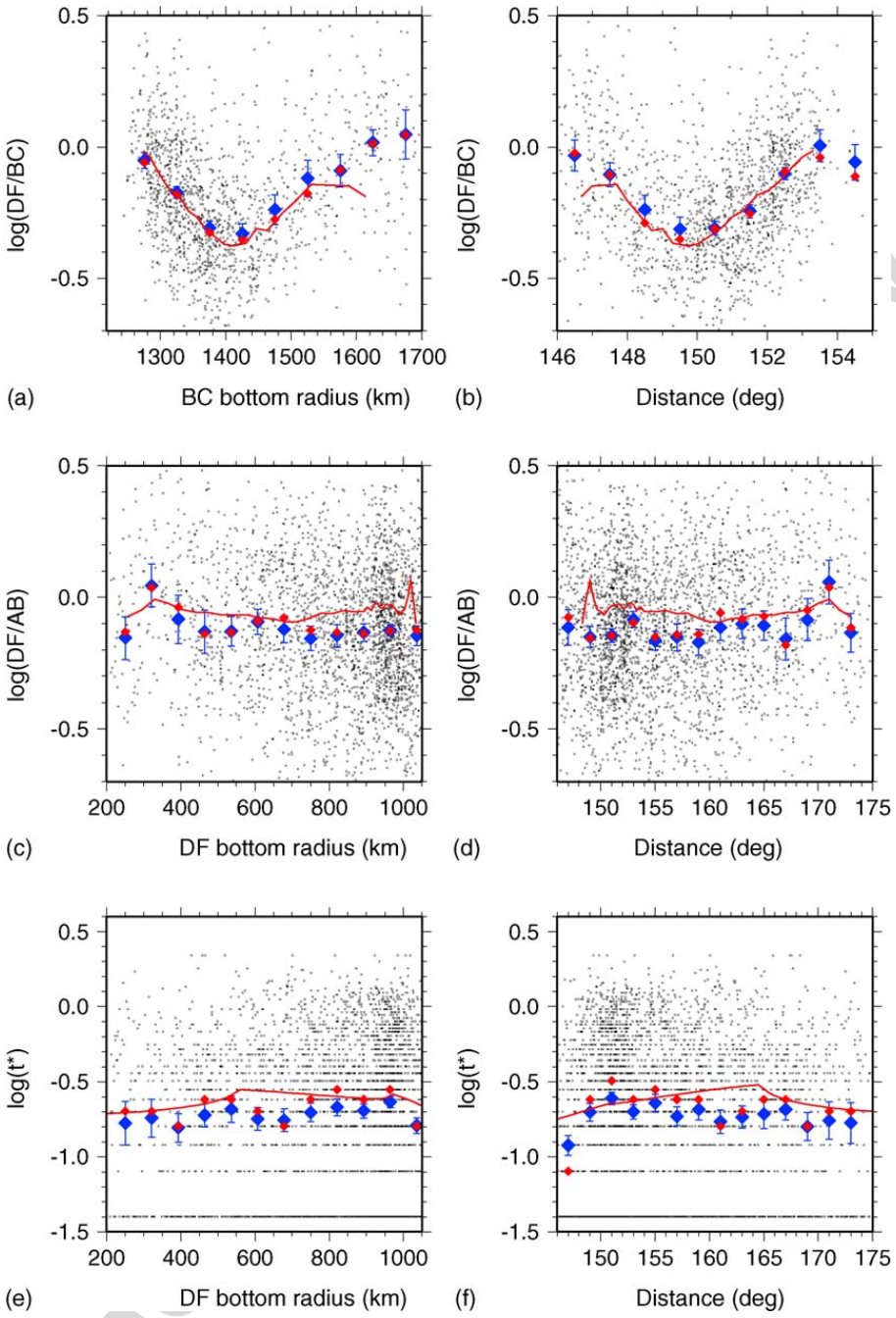

Fig. 11. Logarithm of DF/BC amplitude ratios as a function of PKPbc bottoming point radius (a) and as a function of epicentral distance (b). Logarithm of DF/AB amplitude ratios as a function of PKPdf bottoming point radius (c) and as a function of epicentral distance (d). Logarithm of t^* PKPdf attenuation parameter as a function of PKPdf bottoming point radius (e) and as a function of epicentral distance (f). Individual measurements (black dots), averages (blue diamonds with 2σ error bar) and median (red diamonds) in bottoming radius and epicentral distance bins; and best fit synthetic amplitude ratios and t^* values (red line) are presented in the figure.

2002), despite the fact that at higher frequencies this diffraction effect appears at larger epicentral distances. In contrast, the diffraction of PKPab at the CMB does not produce a strong trend in DF/AB amplitude ratios as can be seen in Fig. 11c and d, because it is compensated by the DF attenuation which maintains an almost constant DF/AB amplitude ratio at large epicentral distances.

The t_i^* values are plotted on Fig. 11e and 11f in logarithmic scale. Only a few discrete values were considered in the inversion to improve the efficiency of the algorithm. In general, t_i^* parameters are underestimated owing to their correlation with R_i^{DF}. However, the main variations of inner core attenuation are retrieved: a strong attenuation at epicentral distances smaller than 150°, an

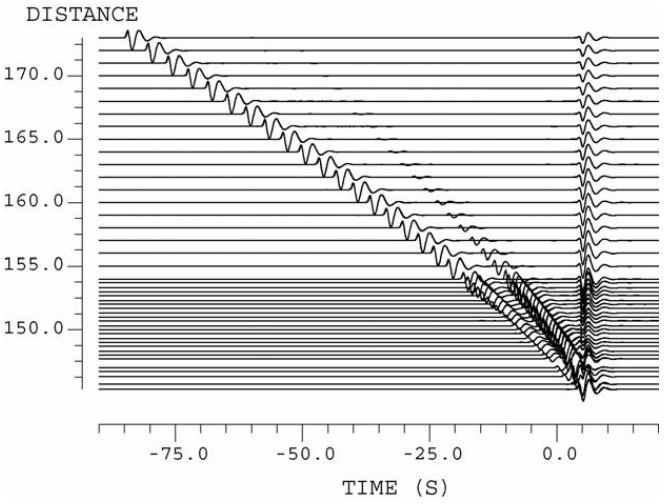

Fig. 12. Full wave theory synthetic PKP waveforms computed for a 300 km deep earthquake in the spherically symmetric ak135 Earth model with an inner core attenuation parameter 1/Q (quality factor Q) values of 0.0035 (285) in the first 250 km of the inner core, 0.003 (330) until 550 km radius, and 0.00001 (100 000) below. Seismic traces are plotted as a function of time (in seconds) and epicentral distance (in degrees). Traces are aligned on PKPab, the reference waveform. The waveform fit by SAWIB is plotted as fine lines but it is almost indistinguishable from the synthetics computed from full wave theory. Note the decrease of PKPbc phase amplitude due to diffraction at the inner core boundary.

almost constant trend in the 150–165° epicentral distance range, and a smaller attenuation for epicentral distances larger than 165°. The good fit of both DF/BC and DF/AB amplitude ratios, and t_i^* is obtained by trial and error, for an inner core attenuation model composed of three layers with attenuation parameter 1/Q (quality factor Q) values of 0.0035 (285) in the first 250 km of the inner core, 0.003 (330) down to 550 km radius, and 0.00001 (100 000) below. Despite its non-uniqueness and its large uncertainties, this model is in good agreement with previous inner core attenuation models with high attenuation in the top of the inner core and low attenuation below (Doornbos, 1983; Li and Cormier, 2002; Cormier and Li, 2002), and recent observations of near-antipodal P′P′ waves (Tkalčić et al., 2006).

In order to detect longitudinal variations of the upper inner core attenuation and velocity structure, non-polar data ($\xi > 40°$) are selected in the PKPdf ray parameter range 1.58–1.65 s/°, corresponding to a PKPdf bottoming point depth range between 150 and 220 km in the inner core. DF/BC and DF/AB amplitude ratios, t^* values, PKP (bc–df) and PKP (ab–df) differential travel time residuals are plotted as a function of PKPdf bottom point longitude in Fig. 13. For both amplitude ratios and t^* values, a trend is seen with lower attenuation in

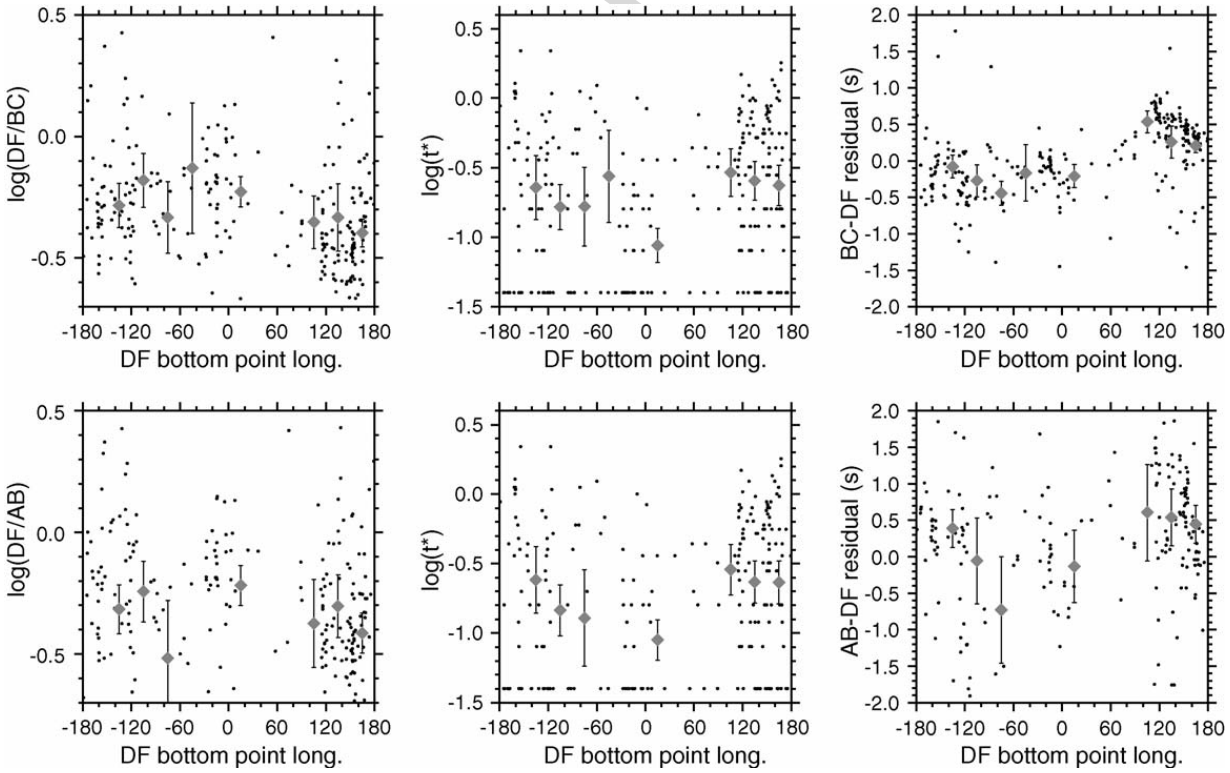

Fig. 13. PKPdf amplitude ratios (left), t^* parameter (middle) and differential travel time residuals (right) relative to PKPbc and PKPab phases respectively for top and bottom panels, as a function of PKPdf bottoming point longitude (in degrees). Only non-polar PKPdf rays ($\xi > 35°$) in the ray parameter range 1.58–1.65 s/° are presented. In this range, PKPdf bottom point depth in the inner core is 150 to 220 km. Black dots are individual measurements, and grey diamonds are logarithmic averages in 30° longitude bins with more than 10 individual measurements and 2σ error bars.

the 180 °W–40 °E longitude range, and higher attenuation in the 40–180 °E range. This result is consistent with a transition between a hemispherical pattern of inner core attenuation in the top 100 km of the inner core (Niu and Wen, 2001; Garcia, 2002; Cao and Romanowicz, 2004), and homogeneous attenuation below (Oreshin and Vinnik, 2004). Moreover, this longitudinal variation is associated with variations in the IC scattering properties with the same longitudinal pattern (Koper et al., 2004; Poupinet and Kennett, 2004). The regions with strong (resp. weak) backscattering at high frequencies are associated with high (resp. low) attenuation of core phases.

A similar hemispherical pattern appears for PKP (bc–df) differential travel time residuals with fast PKPdf rays (positive residuals) in the 40–180 °E longitude range and slow PKPdf rays (negative residuals) in the 180 °W–40 °E longitude range (Shearer and Toy, 1991). PKP (ab–df) differential travel time residuals present noisier results owing to their strong sensitivity to lower mantle heterogeneities, but the results favour a similar hemispherical upper inner core velocity variation.

Taken together, our results favour a hemispherical pattern of both inner core velocity and attenuation. The quasi-eastern hemisphere of the upper inner core in the 40–180 °E longitude range is more attenuating and has faster P-velocities than the quasi-western hemisphere in the 180 °W–40 °E longitude range (Niu and Wen, 2001; Garcia, 2002; Cao and Romanowicz, 2004). The influence of PKPbc diffraction on this hemispherical pattern has been tested in the limit of ±2% of velocity perturbation at the inner core boundary, and it is negligible in the investigated ray parameter range. The hemispherical pattern is partly due to a path from Tonga-Fiji to Europe which presents a strong longitudinal gradient of both differential travel time residuals and amplitude ratios at 180° longitude. With the core phases data set only, it is not possible to discriminate between a transition region in a hemispherical inner core model (Tanaka and Hamaguchi, 1997; Garcia and Souriau, 2000, 2001), lower mantle heterogeneities (Bréger et al., 2000; Tkalčić et al., 2002), or short scale heterogeneities in the upper mantle (Helffrich and Sacks, 1994) along this path. Previous studies have shown that early PKPdf arrivals along polar paths are more attenuated than along equatorial paths, suggesting an anti-correlation between inner core attenuation and inner core anisotropy (Souriau and Romanowicz, 1996; Li and Cormier, 2002; Oreshin and Vinnik, 2004). Our results suggest that the anti-correlation between inner core attenuation and seismic velocities is a general property of the upper inner core along both polar and non-polar rays. If we exclude some rare observations (Kern et al., 1997), Earth materials with high intrinsic attenuation along the fast seismic direction are unknown at upper mantle temperature and pressure conditions. Consequently, such a trend can hardly be explained by intrinsic attenuation. The apparent anisotropy of attenuation has been explained by scattering of seismic waves by small-scale fabric in the inner core (Bergman, 1997; Singh et al., 2000; Cormier and Li, 2002). Singh et al. (2000) proposed that the inner core has a fabric composed of aligned iron crystals responsible for seismic anisotropy, with fluid inclusions at the crystals boundaries, aligned in the equatorial direction, which would explain the anisotropy of attenuation. The decrease of both the inner core attenuation and the anti-correlation between attenuation and wave speed with depth could be explained in such a model by the decrease of the melt fraction (Oreshin and Vinnik, 2004). However, the low amplitude of fast PKPdf rays can also be explained by the de-focusing of body waves propagating along the fast direction of an anisotropic matrix (Samec and Blangy, 1992). In addition to its simplicity, another argument in favour of this explanation is its ability to explain the low dispersion of inner core PKPdf phase observed in studies of inner core attenuation (Li and Cormier, 2002). A complete waveform modelling should be performed in the future in order to quantify the effects of an anisotropic inner core on the amplitude of PKPdf.

5.3. Search for a triplication

The inverted average waveform $W(t)$ provides a good estimate of the source time function, and it can be deconvolved from the data in order to standardize the records of different earthquakes. After alignment on the PKPdf onset, the deconvolved seismograms were stacked in different PKPdf ray parameter bins. This procedure has been applied to the records of deep earthquakes only because their source time function is simpler than for shallow earthquakes, and because they do not suffer of contamination by depth phases. The stacked waveforms are shown in Fig. 14.

In Fig. 14, the diffracted PKPbc phase is seen for PKPdf ray parameters as small as 1.15 s/°, corresponding to an epicentral distance of about 158°. However, we do not detect an additional core phase with a ray parameter close to the one of PKPdf. This result argues against the presence of an innermost inner core discontinuity at global scale, in agreement with other recent studies (Cormier and Stroujkova, 2005; Leyton et al., 2005). Stacks of polar data alone do not preclude the

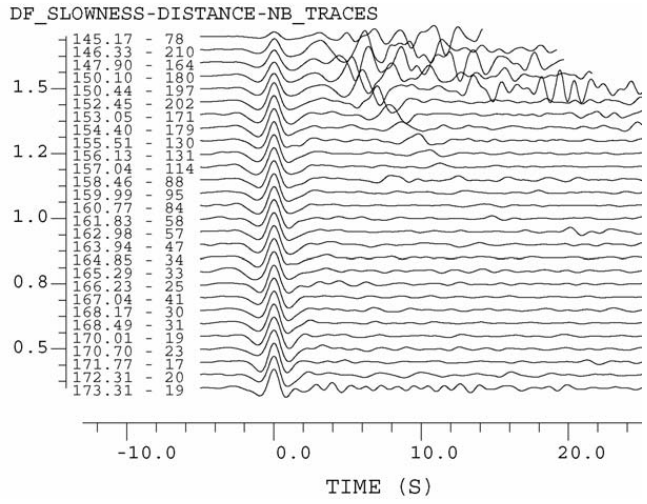

Fig. 14. Stacks of core phase waveforms in different PKPdf ray parameters bins, after deconvolution from the reference waveform, and alignment on the PKPdf arrival. For each stacked trace, the PKPdf slowness (in s/°), the average epicentral distance (in °) and the number of deconvolved traces used for the stack are indicated on the left.

presence of an innermost inner core discontinuity related to anisotropy variations (Ishii and Dziewonski, 2002), because owing to the scarcity of polar paths, the signal to noise ratio in these stacks is rather low.

6. Conclusions

The SAWIB algorithm is an efficient tool for the routine analysis of seismograms in order to measure travel times and amplitudes of body waves, even when different arrivals interfere. The algorithm has been adapted to the processing of PKP phases, including the depth phases for shallow earthquakes. The data from shallow earthquakes provide new paths for probing the deep Earth. The limitations of SAWIB are due to the strong assumptions that are made on the waveforms of the different core phases. In fact, the waveform inversion fails when the waveforms are perturbed by large, small scale heterogeneities at the base of the mantle, or in the crust at the bounce points of the depth phases. As a consequence, SAWIB is best designed to routinely process waveform data in an automated way, but it will not replace full waveform inversion of seismological records. However, our processing of core phases, in addition to other parameters, provides the average waveform of PKP phases, which can be used to compute accurate three-dimensional PKP sensitivity kernels (Calvet and Chevrot, 2005).

The differential travel times PKP (bc–df) and PKP (ab–df) show the same characteristics as previous datasets: a hemispherical variation of average residuals and anomalous polar paths dominated by data from the South Sandwich Island events in the western hemisphere. The differential travel times related to PKPab show a large scatter which likely results from heterogeneities at the base of the mantle.

Diffraction of PKPbc phase at the inner core boundary, and scattering of PKPab at the base of the mantle have clear effects on core phases amplitudes. We demonstrate a decrease of seismic attenuation with depth in the inner core, a property already observed in previous studies. A coarse inner core attenuation model obtained by trial and error explains both the amplitude ratios and the t^* parameters measurements. In this simple three-layer model, the 1/Q (quality factor Q) values are 0.0035 (285) in the first 250 km of the inner core, 0.003 (330) until 550 km radius, and 0.00001 (100 000) below. However, uncertainties and non-uniqueness of the inner core attenuation model should be investigated through more conventional inversion methods in future studies. In the 150–220 km depth range in the inner core, fast rays are more attenuated, and an hemispherical variation of inner core attenuation is observed. The quasi-eastern hemisphere (40–180 °E) is more attenuating than the quasi-western hemisphere (180 °W–40 °E). Because the anti-correlation between seismic velocity and attenuation can hardly be explained by intrinsic attenuation, and because the hemispherical variation of attenuation coincides with the regions where strong scattering has been observed (Koper et al., 2004), a scattering origin for inner core attenuation is favoured in this depth range (Cormier et al., 1998; Singh et al., 2000; Cormier and Li, 2002). However, an alternative explanation is defocusing of PKPdf propagating along fast directions in an anisotropic medium. A complete modeling of the propagation of PKPdf waves in an anisotropic inner core will be crucial to test this hypothesis.

All the deconvolved PKP waveforms were stacked in order to detect any reflection at an innermost inner core discontinuity. We did not detect the presence of a global discontinuity in the inner core, but a discontinuity related to anisotropy variations or to strong local heterogeneities cannot be completely ruled out.

All the results presented here will be improved in the future by keeping accumulating PKP waveform data. This analysis will also be extended to the analysis of other body waves such as P, PcP, PP and Pdiff in order to build the global database necessary for high resolution imaging of the mantle, based on the utilization of finite-frequency Fréchet kernels (Dahlen et al., 2000; Calvet and Chevrot, 2005; Calvet et al., 2006b). Because we can measure the differential travel times and reference waveforms, SAWIB extracts all the information necessary to image the deep Earth structures with 3D sensitivity kernels.

Acknowledgments

We acknowledge all the PASSCAL temporary seismological networks, the seis-mological data centers IRIS and GEOSCOPE, and the following permanent seismological networks available through the NetDC virtual data center. Permanent seismological networks listed in alphabetical order of their abbreviations: AK, AS, AZ, BK, CD, CI, CZ, DW, ER, G, GE, GR, GT, H2, IC, II, IM, IU, KN, KZ, LB, LD, LX, MN, MS, NM, PN, PS, SR, SP, TS, TW, UO, US, UW. A comprehensive list of these networks could be found at www.fdsn.org. This work has been supported by the DyETI program of french Institut National des Sciences de l'Univers. Part of H. T. time was supported by Postdoctoral Program at LLNL. IPGP contribution number 2140.

References

Andresen, B., Gordon, J.M., 1994. Constant thermodynamic speed for minimizing entropy production in thermodynamic processes and simulated annealing. Phys. Rev. E 50, 4346–4351.

Bergman, M., 1997. Measurements of electric anisotropy due to solidification texturing and the implications for the Earth's inner core. Nature 389, 60–63.

Bhattacharyya, J., Shearer, P., Masters, G., 1993. Inner core attenuation from short-period PKP (BC) versus PKP (DF). Geophys. J. Int. 114, 1–11.

Bréger, L., Romanowicz, B., Tkalčić, H., 1999. PKP (BC-DF) travel time residuals and short scale heterogeneity in the deep Earth. Geophys. Res. Lett. 26, 3169–3172.

Bréger, L., Tkalčić, H., Romanowicz, B., 2000. The effect of D″ on PKP (AB-BC) travel time residuals and possible implications for inner core structure. Earth Planet. Sci. Lett. 175, 133–143.

Calvet, M., Chevrot, S., 2005. Traveltime sensitivity kernels for PKP phases in the mantle. Phys. Earth Planet. Int. 153, 21–31.

Calvet, M., Chevrot, S., Souriau, A., 2006a. P-wave propagation in transversely isotropic media. I. Finite-frequency theory. Phys. Earth Planet. Int. 156, 12–20.

Calvet, M., Chevrot, S., Souriau, A., 2006b. P-wave propagation in transversely isotropic media. II. Application to inner core anisotropy: effects of data averaging, parametrization and a priori information. Phys. Earth Planet. Int. 156, 21–40.

Cao, A., Romanowicz, B., 2004. Hemispherical transition of seismic attenuation at the top of the Earth's inner core. Earth Planet. Sci. Lett. 228, 243–253.

Chevrot, S., 2002. Optimal waveform and delay time analysis by simulated annealing. Geophys. J. Int. 151, 164–171.

Cormier, V., Choy, G., 1986. A search for lateral heterogeneity in the inner core from differential travel times near PKP-D and PKP-C. Geophys. Res. Lett. 13, 1553–1556.

Cormier, V., Li, X., 2002. Frequency-dependent seismic attenuation in the inner core. 2. A scattering and fabric interpretation. J. Geophys. Res. 107, doi:10.1029/2002JB001796.

Cormier, V., Li, X., Choy, G., 1998. Seismic attenuation of the inner core: viscoelastic or stratigraphic? Geophys. Res. Lett. 25, 4019–4022.

Cormier, V., Richards, P., 1977. Full wave theory applied to a discontinuous velocity increase: the inner core boundary. J. Geophys. 43, 3–31.

Cormier, V., Stroujkova, A., 2005. Waveform search for the innermost inner core. Earth Planet. Sci. Lett. 236, 96–105.

Creager, K., 1992. Anisotropy of the inner core from differential travel times of the phases PKP and PKIKP. Nature 356, 309–314.

Dahlen, F., Hungh, S.-H., Nolet, G., 2000. Fréchet kernels for finite-frequency traveltime. I. Theory. Geophys. J. Int. 141, 175–203.

Doornbos, D., 1983. Observable effects of the seismic absorption band in the Earth. Geophys. J. R. Astr. Soc. 75, 693–711.

Dziewonski, A., Woodhouse, J., 1983. An experiment in the systematic study of global seismicity: centroid-moment tensor solutions for 201 moderate and large earthquakes of 1981. J. Geophys. Res. 88, 3247–3271.

Engdahl, E., Van der Hilst, R., Buland, R., 1998. Global teleseismic earthquake relocation with improved travel times and procedures for depth determination. Bull. Seismol. Soc. Am. 88, 722–743.

Garcia, R., 2002. Constraints on upper inner core structure from waveform inversion of core phases. Geophys. J. Int. 150, 651–664.

Garcia, R., Chevrot, S., Weber, M., 2004. Nonlinear waveform and delay time analysis of triplicated core phases. Geophys. J. Int. 109, doi:10.1029/2003JB002429.

Garcia, R., Souriau, A., 2000. Inner core anisotropy and heterogeneity level. Geophys. Res. Lett. 27, 3121–3124.

Garcia, R., Souriau, A., 2001. Correction to: inner core anisotropy and heterogeneity level. Geophys. Res. Lett. 28, 85–86.

Garnero, E., Jeanloz, R., 2000. Fuzzy patches on the Earth's core-mantle boundary. Geophys. Res. Lett. 27, 2777–2780.

Garnero, E., Revenaugh, J., Williams, Q., Lay, T., Kellog, L., 1998. Ultra low velocity zone at the core-mantle boundary. In: Gurnis, M., Wysession, M., Knittle, E., Buffett, B. (Eds.), The Core-Mantle Boundary Region. American Geophysical Union.

Gutenberg, B., Richter, C., 1938. P′ and the Earth's core. Mon. Not. R. Astr. Soc. Geophys. Suppl. 4, 363.

Helffrich, G., Kaneshima, S., Kendall, J.-M., 2002. A local, crossing path study of attenuation and anisotropy of the inner core. Geophys. Res. Lett. 29, 9.1–9.4.

Helffrich, G., Sacks, S., 1994. Scatter and bias in differential PKP travel times and implications for mantle and core phenomena. Geophys. Res. Lett. 21, 2167–2170.

Ishii, M., Dziewonski, A., 2002. The innermost inner core of the Earth: evidence for a change in anisotropic behavior at the radius of about 300 km. Proc. Natl. Acad. Sci. U.S.A. 99, 14026–14030.

Kennett, B., Engdahl, E., Buland, R., 1995. Constraints on seismic velocities in the Earth from traveltimes. Geophys. J. Int. 122, 108–124.

Kern, H., Liu, B., Popp, T., 1997. Relationship between anisotropy of P and S wave velocities and anisotropy of attenuation in serpentinite and amphi-bolite. J. Geophys. Res. 102, 3051–3065.

Kolaf, P., 2000. Two attempts of study of seismic source from teleseismic data by simulated annealing non-linear inversion. J. Seism. 4, 197–213.

Koper, D., Franks, J., Dombrovskaya, M., 2004. Evidence for small-scale heterogeneities in the earth's inner core from a global study of pkikp coda waves. Earth Planet. Sci. Lett. 228, 227–241.

Lehmann, I., 1936. P′. Bur. Cent. Seismol. Int. Trav. Sci. A 14, 3–31.

Leyton, F., Koper, K., Zhu, L., Dombrovskaya, M., 2005. On the lack of seismic discontinuities within the inner core. Geophys. J. Int. 162, 779–786.

Li, X., Cormier, V., 2002. Frequency-dependent seismic attenuation in the inner core. 1. A viscoelastic interpretation. J. Geophys. Res. 107, doi:10.1029/2002JB001795.

Morelli, A., Dziewonski, A., Woodhouse, J., 1986. Anisotropy of the inner core inferred from PKIKP travel times. Geophys. Res. Lett. 13, 1545–1548.

Ni, S., Tan, E., Gurnis, M., Helmberger, D., 2002. Sharp sides to the African superplume. Science 296, 1850–1852.

Niazi, M., Johnson, L., 1992. Q in the inner core. Phys. Earth Planet. Int. 74, 55–62.

Niu, F., Wen, L., 2001. Hemispherical variations in seismic velocity at the top of the Earth's inner core. Nature 410, 1081–1084.

Nulton, J., Salamon, P., 1988. Statistical mechanics of combinatorial optimization. Phys. Rev. A 37, 1351–1356.

Oreshin, S., Vinnik, L., 2004. Heterogeneity and anisotropy of seismic attenuation in the inner core. Geophys. Res. Lett. 31, doi:10.1029/2003GL018591.

Poupinet, G., Kennett, B., 2004. On the observation of high frequency PKiKP and its coda in Australia. Phys. Earth Planet. Int. 46, 497–511.

Poupinet, G., Pillet, R., Souriau, A., 1983. Possible heterogeneity of the Earth's core deduced from PKIKP travel times. Nature 305, 204–206.

Romanowicz, B., Tkalčić, H., Bréger, L., 2003. On the origin of complexity in PKP travel time data from broadband records. In: Dehant, V., Creager, K., Karato, S., Zatman, S. (Eds.), Earth's Core: Dynamics, Structure and Rotation. American Geophysical Union, doi:10.1029/031GD04.

Sacks, I., Snoke, J.L.B., 1979. Lateral heterogeneity at the base of the mantle revealed by observations of amplitudes of PKP phases. Geophys. J. R. Astr. Soc. 86, 801–814.

Salamon, P., Berry, R., 1983. Thermodynamic length and dissipated availability. Phys. Rev. Lett. 51, 1127–1130.

Samec, P., Blangy, J., 1992. Viscoelastic attenuation, anisotropy, and AVO. Geophysics 57, 441–450.

Sen, M., Stoffa, P., 1995. Global optimization methods in geophysical inversion. Elsevier.

Sharma, S., Kaikkonen, P., 1998. Two-dimensional non-linear inversion of VLF-R data using simulated annealing. Geophys. J. Int. 133, 649–668.

Shearer, P., Toy, K., 1991. PKP (BC) versus PKP (DF) differential travel times and aspherical structure in the Earth's inner core. J. Geophys. Res. 96, 2233–2247.

Singh, S., Taylor, M., Montagner, J.-P., 2000. On the presence of fluid in the Earth's inner core. Science 287, 2471–2474.

Souriau, A., Romanowicz, B., 1996. Anisotropy in inner core attenuation: a new type of data to constrain the nature of the solid core. Geophys. Res. Lett. 23, 1–4.

Souriau, A., Roudil, P., 1995. Attenuation in the uppermost inner core from broad-band GEOSCOPE PKP data. Geophys. J. Int. 123, 572–587.

Tanaka, S., Hamaguchi, H., 1997. Degree one heterogeneity and hemispherical variation of anisotropy in the inner core from PKP (BC)-PKP (DF) times. J. Geophys. Res. 102, 2925–2938.

Tkalčić, H., Flanagan, M., Cormier, V., 2006. Onservation of near-podal seismic P′P′ precursors: evidence for back scattering from the 150 to 220 km zone in the Earth's upper mantle. Geophys. Res. Lett. 33, L03305, doi:10.1029/2005GL024626.

Tkalčić, H., Romanowicz, B., Houy, N., 2002. Constraints on D′′ structure using PKP (AB-DF), PKP (BC-DF) and PcP-P traveltime data from broadband records. Geophys. J. Int. 148, 599–616.

Wen, L., Niu, F., 2002. Seismic velocity and attenuation structures in the top of the Earth's inner core. J. Geophys. Res. 107, doi:10.1029/2001JB000170.